国立大学法人
九州工業大学

2024 年 10 月 2 日

最適化したノイズによる
確率共鳴現象と逆確率共鳴現象の転移手法の開発

九州工業大学大学院情報工学研究院物理情報工学研究系の許宗君教授が研究代表を務める非平衡散逸系の研究グループは、ノイズのポジティブ効果として知られる確率共鳴現象*1 と逆確率共鳴現象について、液晶の電気対流系を用いて調査を行いました。両共鳴現象を統一的に制御することで、さまざまな応用研究においてシステムのパフォーマンスを柔軟に調整できる可能性が示されています。本研究では、システムの内部パラメータやノイズの特性を定量的に制御することで、両共鳴現象の転移に関わる新たな手法を開発しました。この手法は、ノイズのカラー化やパワースペクトルのエッジ効果、振幅・位相ノイズの混合などを利用しており、バイオテクノロジー、画像処理技術、センサー工学など多くの関連分野への応用が期待されています。

ポイント

- **確率共鳴と逆確率共鳴の転移を示す量(h)を定義する**
- **ノイズの特性と液晶対流系の物性値による h の変化を調査する**
- **特化した振幅ノイズと位相ノイズの絶妙な配合がカギとなる**

普通では検知できない微弱な信号に適切なノイズを加えると、その微弱信号を検出できることがあります。このようなノイズのポジティブ効果は確率共鳴現象として広く知られています。これまで物理系、生物系、情報系、脳科学などの分野で確率共鳴現象（Stochastic Resonance, SR)と逆確率共鳴現象（Inverse

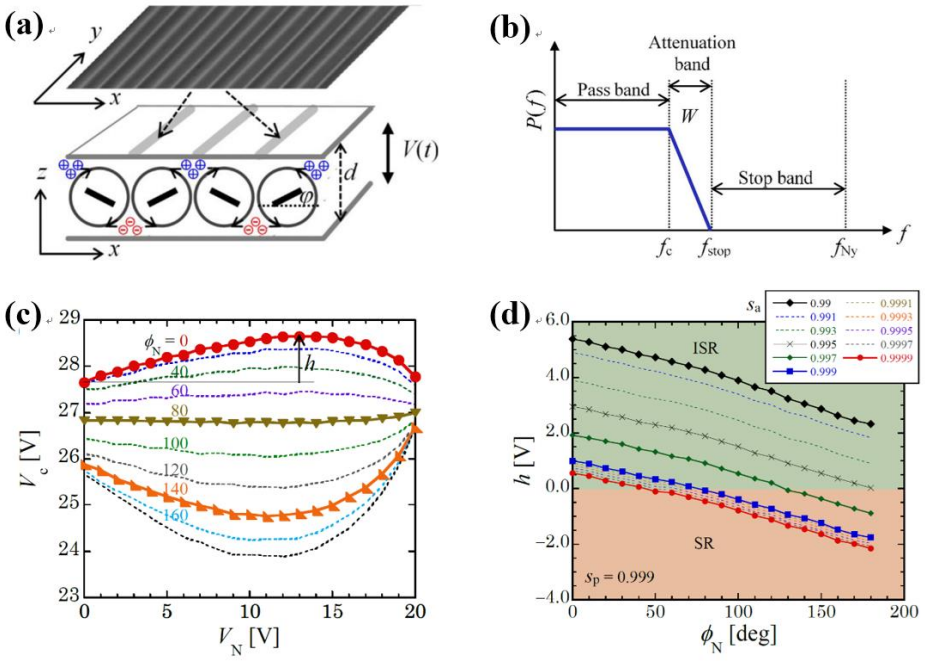

(a)液晶の電気対流系 **(b)**ノイズのパワースペクトル **(c)**両共鳴現象の特性を示す閾値(V_c)の最大値 h の定義。$h>0, h<0$ がそれぞれ ISR と SR を表し、$h=0$ がその転移を表す。**(d)** 位相ノイズのスティープネス（s_p）を固定した状態で、最大値 $h(\phi_N)$を振幅ノイズ s_a で測定。s_a によって、転移（$h=0$）が制御可能。

Stochastic Resonance, ISR）が発見され、応用分野も多岐にわたっています。両共鳴現象の一括制御から必要に応じて系のパフォーマンスを柔軟に制御できる可能性がありますが、今まで SR-ISR の転移を示す実験系の報告例はありませんでした。本研究では世界で初めて数値解析により SR と ISR の転移を捉えた液晶電気対流系*2（図 **a**)に対して、図 **b** に示しているノイズのカラー化（f_c）とパワースペクトルのエッジ効果（W)、振幅・位相ノイズの混合などを定量的に制御しながら SR と ISR の調査を行いました。

調査で用いた液晶の電気対流系はある電圧（V_c）以上で対流が発生します。その交流電界に振幅と位相ノイズを乗せると、図 **c** のように、V_c は大きくなったり小さくなったりします。図 **c** は振幅ノイズ強度 V_N を変えながら V_c の変化を示したグラフであり、その曲線は上から順番に位相ノイズ強度 ϕ_N を強めながら測定した結果です。最大値と最小値を示す非単調なカーブが、それぞれ ISR と S R に相当します。ここで、最大値の高さ h を定義すると、ISR（$h>0$）から SR（$h<0$）への転移（$h=0$）が位相ノイズ ϕ_N によって起きることが分かります。この h を、ノイズの特性の一つであるエッジ効果を表すノイズ・スティープネス（s）で測定した結果、図 **d** のような転移（$h=0$）が分かりました。さらに、液晶対流系の内部パラメータのひとつである液晶の電気伝導度を変えながら h を測定した結果、同様に h の制御が可能であることが分かりました。このような結果は通常のホワイトノイズでは現れません。図 **c** と図 **d** には特化したカラーノイズが極めて重要な役割を果たしています。上述したように、両共鳴現象に敏感かつ制御しやすい内部パラメータ（本研究では電気伝導度）を特定することも、これからの他分野での応用研究において示唆することが多くあります。

この研究成果は、2024 年 9 月 18 日（水）に英国の科学オープンアクセス誌「Scientific Reports (Springer Nature 社)」に掲載されました。

*1 確率共鳴現象：非線形システムにおいて、外部の確率的なノイズが存在する条件下で、システムの性能や感度が最適になる現象を指します。具体的には、確率的なノイズがシステムに追加されると、システムの出力が増幅され、信号検出や情報伝達などのタスクに対する性能が向上することがあります。
*2 液晶電気対流系：液晶層内の電場が十分に強い場合、クーロン力が液晶の粘弾性力に打ち勝ち系内に不安定性が引き起こされ、異方性流体（液晶）の運動が誘発される現象を示すシステムです。

■論文の詳細情報

タイトル：　Manipulating conductivity and noise for transitioning between stochastic and inverse stochastic resonances in liquid–crystal electroconvection
著 者 名：　Jong-Hoon Huh, Takumu Higashi, Yuki Sato
雑　　誌：　Scientific Reports (Springer Nature 社)
D　O　I：　https://doi.org/10.1038/s41598-024-71897-z
※本研究は JSPS 科研費 JP18K03464, JP22K03470 の助成を受けたものです。

【研究内容に関するお問い合わせ】
九州工業大学 大学院情報工学研究院 物理情報研究系教授 許宗煮
電話：0948-29-7897　Mail：huh@phys.kyutech.ac.jp

【報道に関するお問い合わせ】
九州工業大学 経営戦略室
電話：093-884-3007　Mail：pr-kouhou@jimu.kyutech.ac.jp

scientific reports

Check for updates

OPEN

Manipulating conductivity and noise for transitioning between stochastic and inverse stochastic resonances in liquid–crystal electroconvection

Jong-Hoon Huh✉, Takumu Higashi & Yuki Sato

Noise can play a constructive role in nature and various engineering systems. Over the past four decades, noise-induced stochastic resonances (SRs) have been extensively documented, showing enhancement in system performance. Additionally, inverse SR has been observed in various systems. Typically, these resonances were studied independently. A transition between these resonances was recently observed in an alternating current-driven liquid–crystal electroconvection (EC) system using combined amplitude and phase noises. This study uses internal (material) and external (noise) parameters to demonstrate the control of this transition. Specifically, the nonmonotonic threshold voltage behavior of the EC system, indicative of the resonances, was numerically examined using additional parameters. Experimental tests were conducted to confirm the effects of these parameters. The findings reveal that the transition between these resonances can be systematically controlled to meet specific needs, whether desirable or undesirable system performances. Notably, this study illustrates how to modify the behavior of both resonances in colored noise by adjusting its cutoff frequency and steepness and phase noise, which is often overlooked. Moreover, this study provides valuable insights for various noise-related applications.

Noise-induced stochastic resonance (SR) and inverse stochastic resonance (ISR) are intriguing counterintuitive phenomena[1,2]. SR is characterized by a bell-shaped signal-to-noise ratio (SNR) curve, indicating optimal output performance at a specific noise intensity. In contrast, ISR decreases performance, resulting in an inverted bell-shaped SNR curve. Benzi et al. first proposed SR and its underlying mechanism in the context of ice-age cycles[1,3]. Since then, SR has been extensively studied in various fields, including electronic devices[4,5], nonlinear chemical reactions[6,7], reaction mechanisms of living organisms[8,9], image processing[10,11], and neural networks[12,13]. Similarly, since the first identification of ISR in a neural network system[2,14,15], it has been reported in other systems, such as ecological systems[16] and electroconvection (EC) systems[17]. However, in most studies[1–17], these resonances have been investigated separately. A recent study[18] discovered a substantial transition between SR and ISR in a liquid–crystal EC system using specific combinations of amplitude and phase noises.

Generally, a weak deterministic signal and a double minimum potential function $U(x)$ are crucial for the generation of SR and ISR[19–21]. Additionally, it is essential that the reflection symmetry ($x \rightarrow -x$) of the double minimum potential is broken for both resonances[20]. Previous studies[19–21] found that the symmetry-broken potential is periodic and stationary for SR and ISR, respectively. For both resonances, additive noise and multiplicative noise have been employed[21,22]; additive noise is independent of the variable indicating output performance [21–23], while multiplicative noise is coupled to the variable (e.g., ψ in Eqs. (1) and (2))[24,25]. Moreover, most earlier studies[1,3,6,9,10,12] used white noise to generate both resonances. However, colored noise was found to be essential for controlling their generation[17,18,21–25]. Notably, colored noise with a finite autocorrelation time ($\tau_c \neq 0$) can be distinguished from conventional white noise ($\tau_c = 0$)[18,21,26]. Typically, amplitude noise has been used for both resonances; however, phase noise, which is often overlooked, was found to contribute to SR in a nanoelectromechanical membrane system[27] and EC systems[28]. Additionally, Gaussian noise has usually been employed for both resonances[1–28], but SR has also been observed in non-Gaussian noise[29,30]. Amplitude and phase noises that

Department of Physics and Information Technology, Faculty of Computer Science and Systems Engineering, Kyushu Institute of Technology, Fukuoka 820–8502, Japan. ✉email: huh@phys.kyutech.ac.jp

are multiplicative, colored, and of Gaussian-type were used in this study. The degree of colorization of both noises, which is controlled by the autocorrelation time and the steepness of their power spectra, is particularly important in this investigation[18,26,31].

In a recent report[18], SR and ISR in the EC system (Fig. 1a) were investigated using numerical calculations of the threshold voltage V_c of the alternating current (AC)-driven EC. The emergence of both resonances was also experimentally confirmed in the EC system[17,18,28]. It was discovered that amplitude noise-induced ISR[17] and phase noise-induced SR[28] in the EC system combined in the presence of both noises, revealing a transition between the competing resonances[18]. The noise-dependent curves of V_c exhibited bell-shaped and inverted bell-shaped behaviors corresponding to ISR and SR, respectively. Notably, a bell-shaped V_c curve indicates that the output performance (i.e., the growth of EC) shows an inverted bell-shaped SNR curve for ISR[17] and vice versa for SR[28]. Thus, a transition between SR and ISR was first discovered in an actual system[18].

Two meaningful parameters, an internal (material) parameter and an external (noise) parameter, were introduced in this study to deepen the understanding of the transition in the EC system. The first parameter is the Helfrich conductivity σ_H, which is determined by adjusting the electric conductivity of nematic liquid crystals (NLCs)[32]. It can be experimentally realized by doping a compound, for example, tetrabutylammonium bromide (TBAB), into n-(4-methoxybenzylidene)-4-butylaniline (MBBA), as used in this study[26] (see Eq. (1)). The second parameter is the steepness of the noise power spectra $P(f)$, defined by the attenuation (frequency) band, as shown in Fig. 1b [31]. A cutoff frequency f_c of the noise in Fig. 1b is defined to characterize colored noise using a low-pass filter[26]. Subsequently, noise with pass-band frequency components (i.e., $f<f_c$) is generated and used as

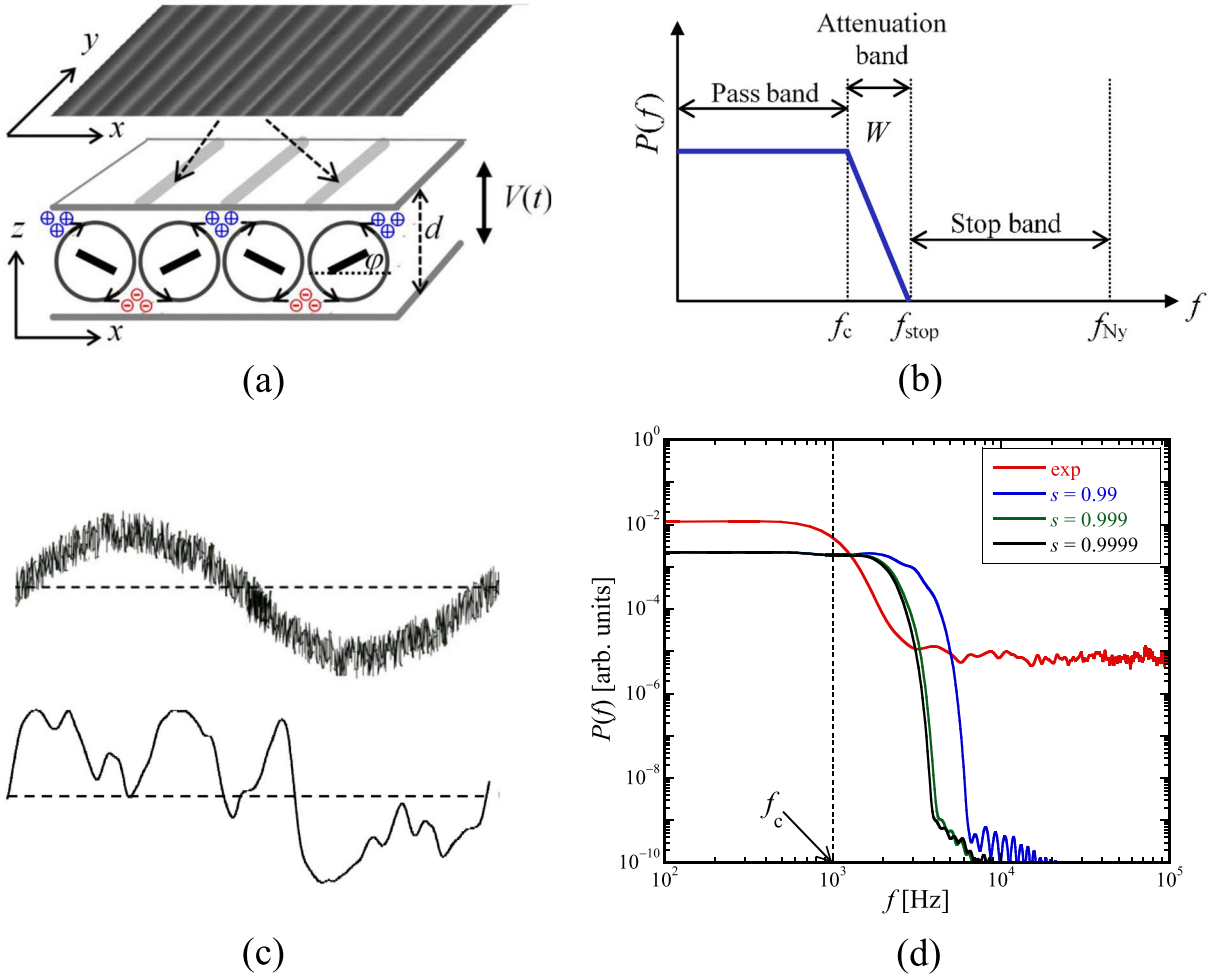

Fig. 1. AC-driven electroconvection (EC) with superposed external colored noise. (**a**) Schematic of EC driven by Coulomb forces on electric charges (+,−) in a nematic liquid crystal (NLC). The rods in the EC vortices indicate the director $\mathbf{n}(n_x, 0, n_z)$ of the NLC modulated from the initial director $\mathbf{n}_0 = (1, 0, 0)$ (at $V = 0$). Above a threshold voltage V_c, EC is optically observed as a periodic roll pattern (i.e., the so-called Williams domains) in the xy plane by the lens effect of the periodic director angle $\varphi(x)$. (**b**) Power spectra $P(f)$ of colored noise characterized by the cutoff frequency f_c of the pass band and the width W of the attenuation band. (**c**) Schematic of Gaussian amplitude noise (top) and phase noise (bottom) superposed on a sinusoidal AC signal. (**d**) Typical $P(f)$ of noise in this study, characterized by the steepness s corresponding to W at a fixed f_c; note that $s = 1$ indicates $W = 0$ for ideal noise filters. Each $P(f)$ was obtained from the noises generated by a frequency filtering program integrated into the general-purpose software (MATLAB). Compare these $P(f)$ from the filtering program with that ($s = 0.80$) obtained experimentally from a wave generator (HIOKI, 7075).

a superposing noise to the EC system. In principle, the ideal low-pass filter has no attenuation band (i.e., $W=0$), but real noises are experimentally and numerically generated with it (i.e., $W\neq 0$)[26,31]. Generally, the steepness s of colored noise is defined as $W=(1-s)(f_{Ny}-f_c)$, using a Nyquist frequency f_{Ny}[33]. Thus, $s=1$ indicates the ideal cutoff frequency of an ideal low-pass filter (i.e., $W=0$). The steepness s is first introduced to investigate the transition between both resonances. Specifically, two kinds of steepness, i.e., amplitude noise (i.e., s_a) and phase noise (i.e., s_p), are utilized in this study. The sinusoidal signals superposed by amplitude and phase noises must be noted (Fig. 1c). The power spectra $P(f)$ of noise with different steepness in Fig. 1d are provided to confirm feature of the steepness. Evidently, the attenuation band changes with the steepness variation. Additionally, this study explored whether the attenuation frequencies varied by steepness can play a role in the occurrence of EC and the emergence of both resonances. Expanding SR and ISR into advanced applications necessitates controlling both resonances. Therefore, based on actual needs, one subsequently controls desired and undesired system performances from this idea. For instance, a desired effect (of SR) and an undesired side effect (of ISR) in actual applications may be controlled by employing such internal and external parameters of the system of interest.

In this numerical study, the threshold voltage V_c for the EC system was calculated using the one-dimensional Carr–Helfrich equations (Eqs. (1) and (2)) for an NLC, specifically MBBA, sandwiched between two parallel electric plates with a gap distance d[32,34]:

$$\dot{q}+\frac{q}{\tau}+\sigma_H\frac{V(t)}{d}\psi=0, \tag{1}$$

$$\dot{\psi}+\lambda\left[E_0^2+\left(\frac{V(t)}{d}\right)^2\right]\psi+\frac{q}{\eta}\frac{V(t)}{d}=0, \tag{2}$$

where $q(t)$ and $\psi(t)$ represent the space-charge density and the variation of the director ($\psi=\partial\varphi/\partial x$), respectively (Fig. 1a). Generally, the director $\boldsymbol{n}$ is defined by a unit vector indicating the locally averaged direction of the rodlike molecules in NLCs[32]. In principle, the Carr–Helfrich effect causes electrohydrodynamic instability for $V>V_c$, providing a periodic deviation angle $\varphi(x)$ from the homogeneous initial director $\boldsymbol{n}_0$ [$=(1,0,0)$ at $V=0$][32]. As a result, a well-ordered convection structure called Williams domains (Fig. 1a) can be observed through a lens effect due to the director modulation[32,35]. In other words, EC arises at the transition from $\varphi=0$ (for $V<V_c$) to $\varphi\neq 0$ (for $V>V_c$). Therefore, V_c can be determined as the lowest voltage in the numerical loop with an increment of ΔV, at which the director angle φ does not relax to zero[36]. Furthermore, the dielectric constant ε and electric conductivity σ define the Helfrich conductivity in Eq. (1) as $\sigma_H=\sigma_\parallel(\varepsilon_\perp/\varepsilon_\parallel-\sigma_\perp/\sigma_\parallel)$, where the subscripts $\parallel$ and $\perp$ indicate the directions parallel and perpendicular to the initial director $\boldsymbol{n}_0$, respectively[32,34]. Additionally, material parameters, such as the electric and viscoelastic properties of NLCs, determine the values of τ, λ, E_0^2, and η[32,36]. In the absence of noise, the threshold voltage V_c of EC is analytically determined as follows[32,36]:

$$V_c^2(f)=\frac{V_0^2(1+4\pi^2f^2\tau^2)}{\delta^2-(1+4\pi^2f^2\tau^2)}, \tag{3}$$

where V_0 represents a specific voltage ($V_0=E_0d$) at an AC frequency f and δ is a dimensionless coefficient influenced by the material properties of the NLC. Typically, V_0 ranges from 10 to 25 V, and $1.5<\delta^2<4$ for MBBA, as used in this study[36].

Additionally, in the presence of conventional white amplitude noise [i.e., $\xi_a(t)$ in $V(t)=\sqrt{2}V\cos(2\pi ft)+A_N\xi_a(t)$], the threshold voltage V_c can be analytically determined as follows[34]:

$$V_c^2(f,V_N)=V_{c0}^2+b(f)V_N^2, \tag{4}$$

$$b(f)=\frac{1+4\pi^2f^2\tau^2}{\delta^2-(1+4\pi^2f^2\tau^2)}, \tag{5}$$

where V_{c0} represents the threshold voltage when the noise intensity $V_N=\sqrt{<(A_N\xi_a(t))^2>}=0$. Previous studies[37,38] indicate that parameter b has a positive value for white noise but can be negative for properly adjusted colored noise. Thus, for colored noise, the noise correlation time τ_c and the charge relaxation time τ should modify b[38]. Technically, the cutoff frequency f_c of low-pass filters (where $f_c=1/(2\pi\tau_c)$) can control τ_c[26,38]. Under these noise conditions, the function $V_c(V_N)$ exhibits a monotonic behavior [Eq. (4)], showing no SR or ISR that appear in the nonmonotonic behavior of $V_c(V_N)$. Occasionally, experiments with uncontrolled material properties and noises have shown the nonmonotonic behavior of $V_c(V_N)$, although SR and ISR were not mentioned in those studies[26].

Considering the Helfrich conductivity σ_H of EC and the steepness s of noise, the behavior of V_c in the presence of well-adjusted noises was examined. Numerical calculations were performed using an electric voltage $V(t)$ with both amplitude and phase noises as follows[18]:

$$V(t)=\sqrt{2}V\cos\left[2\pi ft+\phi_N\xi_p(t)\right]+A_N\xi_a(t), \tag{6}$$

Where $\xi_a(t)$ and $\xi_p(t)$ correspond to the amplitude and phase Gaussian-colored noises with steepness ($s\neq 1$), respectively, and ϕ_N indicates the intensity of the phase noise ($0\leq\phi_N\leq 180$ degrees). Amplitude and phase noises were adjusted by setting specific values for s ($0.9<s<1$) and f_c. The conditions of $f_{ca}=1$ kHz and $f_{cp}=50$ Hz, representing the cutoff frequencies of the amplitude and phase noises, respectively, were fixed in this study for the

numerical calculations. Indeed, s and f_c can be determined using a built-in frequency filtering program integrated within the software (MATLAB solver) used in this study[18]. In a recent study[18], nearly ideal colored noises with $s_a = s_p = 0.999$ were employed in the numerical analysis. While f_c can be controlled experimentally through low-pass filters[18,26], adjusting s experimentally poses challenges.

Results

Control of SR and ISR by the Helfrich conductivity

Based on a recent study utilizing colored amplitude and phase noises[18], SR, ISR, and their transition were quantitatively investigated through numerical calculations of the threshold voltage V_c. A typical result of V_c from a recent report[18] is presented in Fig. 2a to provide a clearer understanding of the current findings. In this result, obtained under fixed conditions (i.e., $f = 2.5$ kHz, $f_{cp} = 50$ Hz, $f_{ca} = 1$ kHz, $s_a = s_p = 0.999$, and $\sigma_H = 1.52 \times 10^{-8}\Omega^{-1}$ m^{-1}), V_c varies with the amplitude noise intensity V_N in a smooth manner, correlating with the phase noise intensity ϕ_N. For instance, the bell-shaped curve of $V_c(\phi_N = 0)$, indicating ISR, transitions into a monotonic curve ($\phi_N = 80$ degrees) with nearly the same value and further transitions into an inverted bell-shaped curve of $V_c(\phi_N > 80$ degrees), indicating SR (e.g., $\phi_N = 140$ degrees). Hereafter, the units of ϕ_N [degrees] and σ_H [$10^{-8}\Omega^{-1}$ m^{-1}] are omitted for convenience.

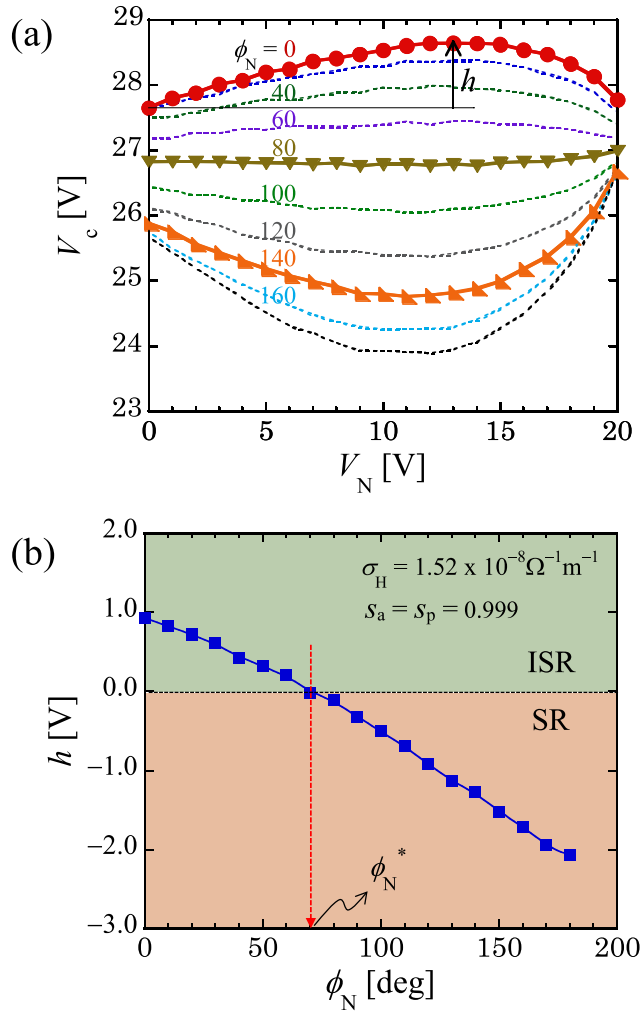

Fig. 2. Behavior of the EC threshold voltage V_c in relation to amplitude noise intensity V_N and phase noise intensity ϕ_N. (**a**) Behavior of $V_c(V_N)$ for different values of ϕ_N. Note that a bell-shaped curve of V_c (e.g., $\phi_N = 0$) changes into an inverted bell-shaped curve (e.g., $\phi_N = 140$ deg); the former and the latter indicate ISR and SR, respectively. (**b**) The height h, indicating the degree of the output performance of SR or ISR, was extracted from (**a**). Accordingly, $h = 0$ means that the performance of SR or ISR completely fades out. A characteristic phase noise intensity ϕ_N^* (~70 deg) can be determined for $h = 0$. The data were obtained at the following fixed values: $f = 2.5$ kHz for EC, $f_{ca} = 1$ kHz, $f_{cp} = 50$ Hz, and $s_a = s_p = 0.999$ for noise, and the Helfrich conductivity $\sigma_H = 1.52 \times 10^{-8}\Omega^{-1}$ m^{-}. For convenience, the units of σ_H [$10^{-8}\Omega^{-1}$ m^{-1}] are omitted in the captions of Figs. 3, 4, and 9.

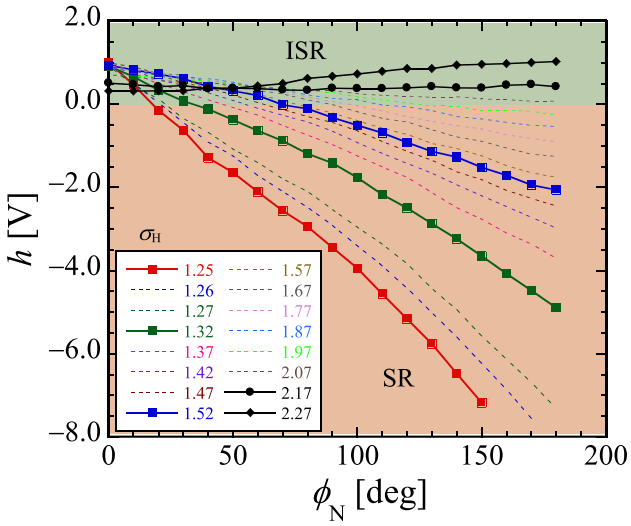

Fig. 3. Height h as a function of phase noise intensity ϕ_N for different values of σ_H. Note that the curve of $h(\phi_N)$ for $\sigma_H = 1.52$ is the same as in Fig. 2b. The regions where $h > 0$ and $h < 0$ indicate ISR and SR, respectively. Thus, the characteristic phase noise intensity ϕ_N^* for $h = 0$ is determined for each value of σ_H. However, no ϕ_N^* is found, because $h > 0$ for all values of ϕ_N. This means that the transition from ISR to SR does not occur. The data were obtained under the same conditions as in Fig. 2, except for σ_H.

To elucidate the characteristics of SR and ISR, h is introduced as the height of the bell-shaped curve, as depicted in Fig. 2a. Here, $h = V_c(V_N = V_N^*) - V_c(V_N = 0)$ at a specific intensity V_N^*, where V_c attains maximal (for ISR) or minimal (for SR) values. Accordingly, with $h > 0$ and $h < 0$ indicating ISR and SR, respectively, the transition from ISR to SR occurring at a characteristic phase noise intensity ϕ_N^* (approximately 80 in Fig. 2a) can be assessed, where h approaches 0 (i.e., the disappearance of ISR and the onset of SR). Clearly, Fig. 2b illustrates a distinct transition between SR and ISR, as extracted from Fig. 2a. It is noteworthy that ISR ($h > 0$) transitions into SR ($h < 0$) at ϕ_N^* when $h = 0$. The more precise value of ϕ_N^* (approximately 70) can be observed in Fig. 2b. Moreover, apart from the transition ($h = 0$), the magnitude of $|h|$, which corresponds to maximal or minimal SNR, can be regulated. This highlights the influence of noise on the desirable or undesirable output performance for practical applications within the system of interest.

To comprehend the responses of both resonances to changes in the internal properties of EC, this study analyzed the threshold function $V_c(V_N)$ as a function of the Helfrich conductivity σ_H under fixed external conditions of amplitude and phase noises, with $s_a = s_p = 0.999$. An AC frequency $f = 2.5$ kHz was employed for EC, maintaining consistency with the conditions depicted in Fig. 2a, extracted from a recent report[18]. Following the derivation of $V_c(V_N)$ illustrated in Fig. 2a, the function $h(\phi_N)$ with different values of σ_H was determined, as depicted in Fig. 3. Notably, h increases with increasing ϕ_N for larger σ_H (> 2). In contrast, it decreases for smaller σ_H (< 2). The characteristic intensity $\phi_N^*(h = 0)$ of the phase noise is identified for $\sigma_H < 2$, depending on each value of σ_H, signifying the transition from ISR ($h > 0$) to SR ($h < 0$). Particularly, ISR ($h > 0$) is solely observed for large values of σ_H (> 2). In other words, there is no $\phi_N^*(h = 0)$; for example, refer to $h(\phi_N)$ for $\sigma_H = 2.27$. Consequently, as depicted in Fig. 4, three regions are delineated based on σ_H, including the regions of ISR ($\sigma_H > \sigma_H^{**} \sim 2.05$) and transition from ISR to SR ($\sigma_H^* < \sigma_H < \sigma_H^{**}$) and an unknown region ($\sigma_H < \sigma_H^* \sim 1.15$). Notably, in this unknown region, V_c seems to diverge, exhibiting values of h greater than 100 V (in numerical calculation). Importantly, in the region of the transition from ISR to SR, $\phi_N^*(h = 0)$ increases with increasing σ_H. These findings indicate that the control of the transition from ISR to SR is feasible under limited conditions ($\sigma_H^* < \sigma_H < \sigma_H^{**}$). From an advanced application standpoint, an internal parameter (such as σ_H, which can be altered by electric conductivityσ) can regulate the magnitude of h, indicating the maximal or minimal output performance of application systems, and $h = 0$, indicating the transition between both resonances. Hence, these results offer a pivotal insight into various noise-related applications employing SR and ISR: a controllable (internal) parameter may furnish a more effective control mechanism for the output performance. Thus, it is crucial to identify a parameter that is easily controllable and sufficiently sensitive to the output performance of the system of interest. This study confirmed that the dielectric constants $\varepsilon_{||}$ and $\varepsilon_{\perp}$ are not easily controllable in experimentation and lack the requisite sensitivity for controlling both resonances.

Control of SR and ISR by the steepness of noise power spectra

Similarly, $V_c(V_N)$ was investigated while varying the steepness s of both noises under fixed conditions of $f_{ca} = 1$ kHz and $f_{cp} = 50$ Hz. The parameters $f = 2.5$ kHz and $\sigma_H = 1.52$ were kept constant for the EC. Initially, the function $h(\phi_N)$ was established for different values of s_a for the amplitude noise, with a fixed $s_p = 0.999$ for the phase noise, as illustrated in Fig. 5. It is clear that h decreases almost linearly with increasing ϕ_N, regardless of s_a. Furthermore, the $h(\phi_N)$ curve shifts into lower values with increasing s_a. However, it is observed that for $s_a \leq 0.995$, $h > 0$, exclusively indicating ISR. Consequently, no transition from ISR to SR is discernible under these s_a conditions.

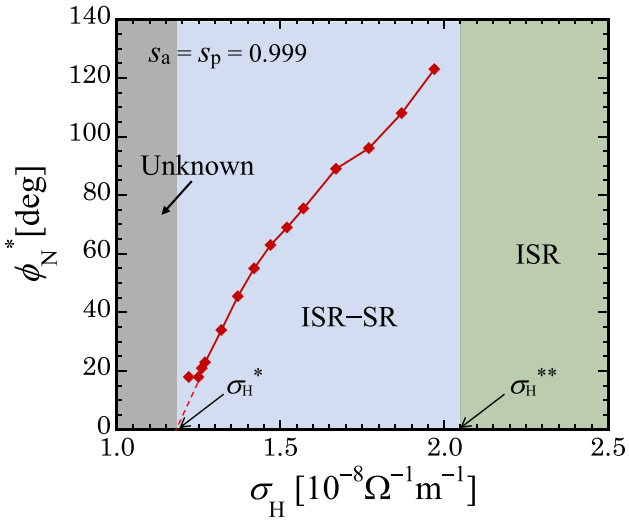

Fig. 4. Three regions of SR and ISR depending on the Helfrich conductivity σ_H. The characteristic phase noise intensity $\phi_N^*(h=0)$ was extracted from $h(\phi_N)$ in Fig. 3. The region of ISR only is speculated for $\sigma_H > \sigma_H^{**} \sim 2.05$, a higher characteristic value of σ_H. However, for $\sigma_H < \sigma_H^* \sim 1.15$, a lower characteristic value of σ_H, h appears to diverge (larger than 100 V in the numerical calculation). Note that the region of the transition from ISR to SR is limited to $\sigma_H^* < \sigma_H < \sigma_H^{**}$.

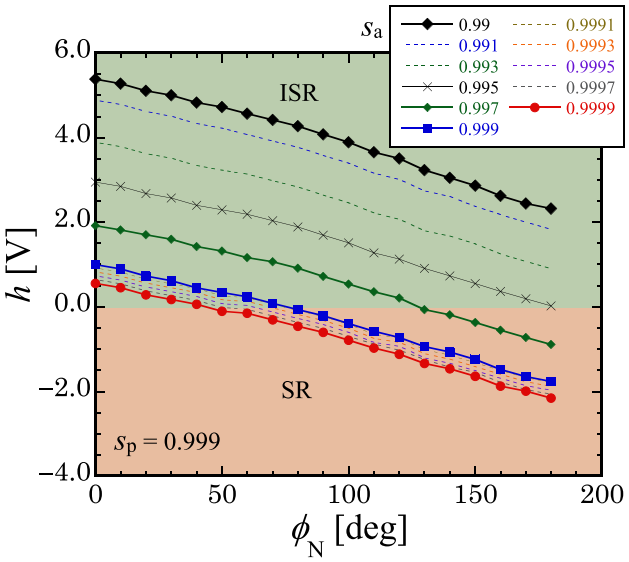

Fig. 5. Height h as a function of phase noise intensity ϕ_N for different values of amplitude noise steepness s_a and a fixed phase noise steepness $s_p = 0.999$. The parameters f, f_{ca}, f_{cp}, and σ_H were fixed at the same values as in Fig. 2b. Notably, h decreases with increasing ϕ_N. Furthermore, this decrease is almost linear and independent of s_p. Only ISR ($h > 0$) is found for values of s_a smaller than the characteristic value $s_a^* \sim 0.995$. In other words, the transition from ISR to SR does not occur. Compare this behavior to that exhibited in Fig. 7.

Thus, the ϕ_N^* characteristic value for $h = 0$ was determined for $s_a > 0.995$. Figure 6 illustrates the behavior of $\phi_N^*(h=0)$, demonstrating a smooth decrease with increasing s_a. The result delineates two regions contingent on s_a: the regions of ISR ($s_a < s_a^* \sim 0.995$) and transition from ISR to SR ($s_a > s_a^*$). Unlike the σ_H-dependent regions depicted in Fig. 4, no region of SR exclusively is identified due to $s \leq 1$.

Next, $h(\phi_N)$ was determined for different values of s_p of the phase noise at a fixed $s_a = 0.999$ of the amplitude noise, as depicted in Fig. 7. The conditions of $f = 2.5$ kHz and $\sigma_H = 1.52$ were also maintained. Similar to $h(\phi_N)$ obtained for different values of s_a (Fig. 5), $h(\phi_N)$ also decreases smoothly with increasing ϕ_N, independent of s_p. In contrast to the findings in Fig. 5, $h(\phi_N)$ shifts to higher values with increasing s_p. Furthermore, $h(\phi_N)$ decreases nonlinearly with increasing ϕ_N for $s_p < 0.999$ and decreases almost linearly with increasing ϕ_N for $s_p \geq 0.999$. Moreover, the transition from ISR ($h > 0$) to SR ($h < 0$) is observed for all values of s_p. In other words, $\phi_N^*(h=0)$

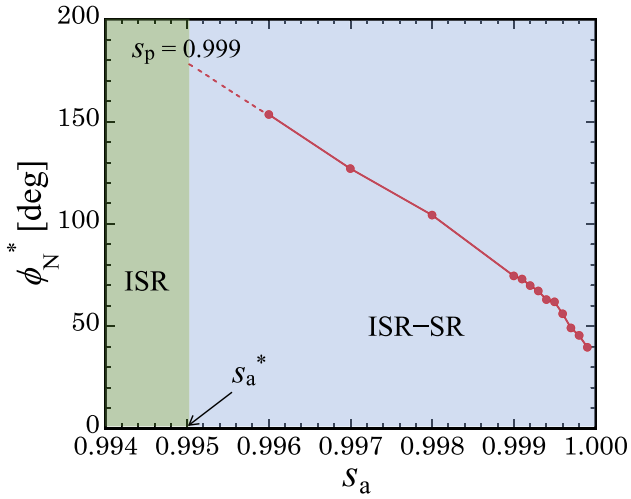

Fig. 6. Two regions of SR and ISR depending on amplitude noise steepness s_a. The characteristic phase noise intensity $\phi_N^*(h=0)$ was extracted from $h(\phi_N)$ in Fig. 5. The region of ISR only is found for $s_a < s_a^* \sim 0.995$, while the region of the transition from ISR to SR is found for $s_a > s_a^*$. Note that no SR region is only found because the maximal value of s_a is 1. Obviously, ϕ_N^* smoothly decreases with increasing s_a. Compare this to the behavior exhibited in Fig. 8.

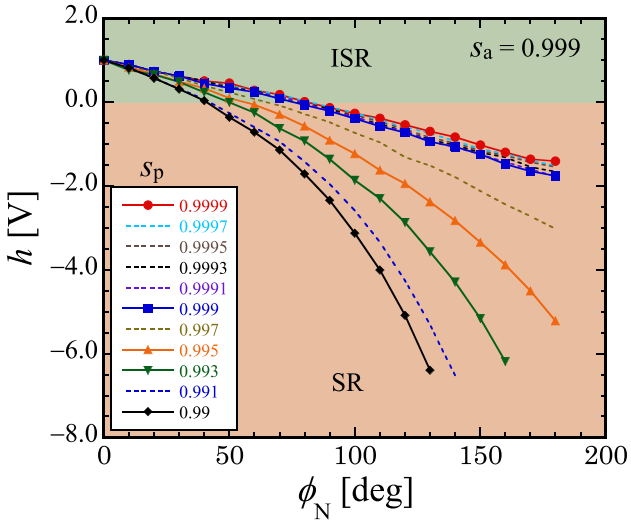

Fig. 7. Height h as a function of phase noise intensity ϕ_N for different values of phase noise steepness s_p and a fixed amplitude noise steepness $s_a = 0.999$. The parameters f, f_{ca}, f_{cp}, and σ_H were fixed at the same values as in Fig. 2b. Similar to Fig. 5, h smoothly decreases with increasing ϕ_N. However, the behavior of $h(\phi_N)$ changes from a linear decrease ($s_p > 0.999$) to a nonlinear one ($s_p < 0.999$). Note that the value of h at $\phi_N = 0$ is fixed ($h \sim 1$ V) because no phase noise was applied, and only amplitude noise was applied. Compare this to Fig. 5, where different amplitude noises with different s_a were applied, resulting in different values of h at $\phi_N = 0$ depending on s_a.

is determined for the transition, independent of s_p. Figure 8 illustrates the behavior of $\phi_N^*(h=0)$, demonstrating an almost exponential increase with increasing s_p. In this scenario, the transition from ISR to SR always occurs for typical colored noises ($s_p > 0.8$) used in experiment. This behavior of $\phi_N^*(s_p)$ is markedly different from that of $\phi_N^*(s_a)$ found in the case of $h(\phi_N, s_a)$ (Fig. 6); the former exhibits a monotonic increase with the steepness s_a, whereas the latter displays a monotonic decrease with s_p. This indicates that the control of the transition from ISR to SR should involve the fine adjustment of the steepness of both noises. From a practical application standpoint, it is crucial to manipulate an external control parameter, such as the steepness of noise power spectra. In most previous studies[17,18,22,23,28,37,38], although colored noise was utilized, only its cutoff frequency was adjusted without defining the steepness. The present results underscore the significance of steepness in controlling both resonances. The steepness function is typically unavailable in experimental setups, even in dedicated noise generators. Nonetheless, confirming the attenuation band is imperative to comprehend the edge effect of noise

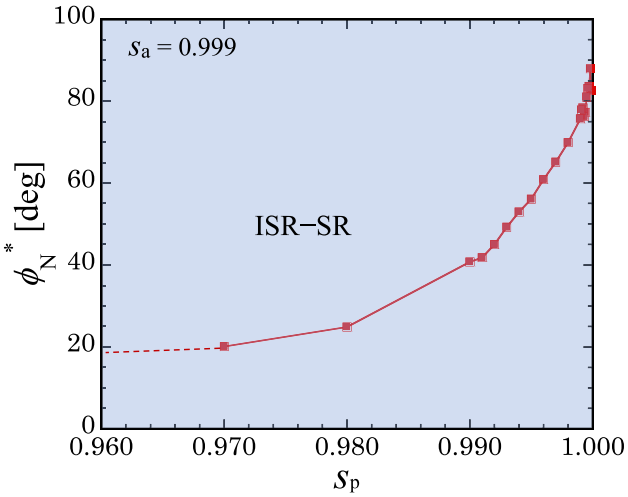

Fig. 8. Transition from ISR to SR concerning phase noise steepness s_p. The characteristic phase noise intensity $\phi_N^*(h=0)$ was extracted from $h(\phi_N)$ in Fig. 7. Considering $h>0$ for $\phi_N=0$ (Fig. 7) and the maximal value $s_p=1$, the regions of SR only or ISR only are not found. Contrary to Fig. 6, ϕ_N^* smoothly increases with increasing s_p.

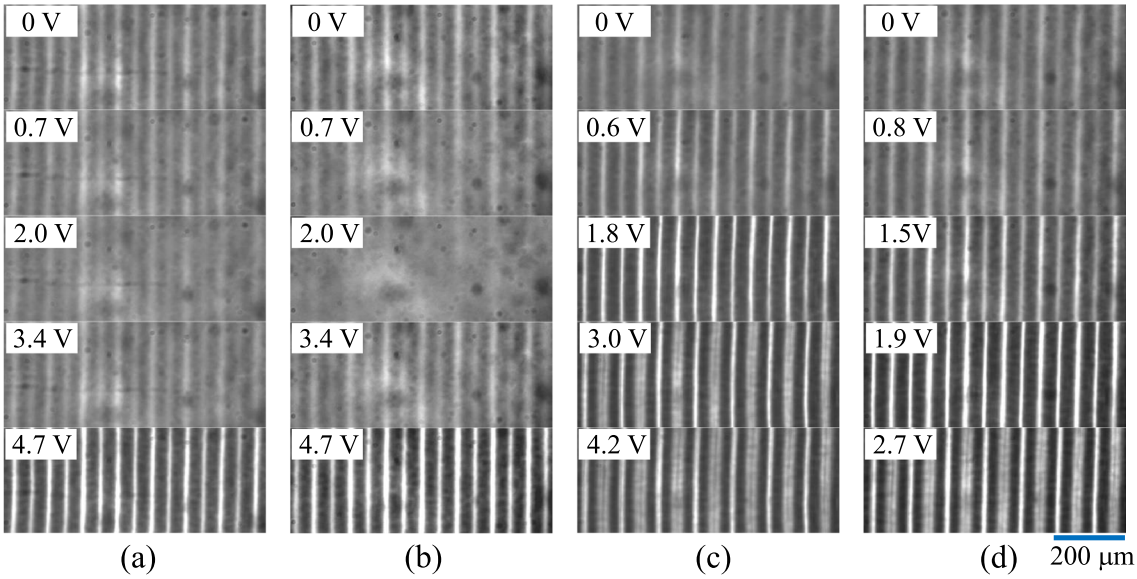

Fig. 9. Experimental tests for the Helfrich conductivityσ_H and noise steepness s_a in an EC ($V=5.9$ V and $f=500$ Hz) conducted in MBBA. Pattern changes indicating the output performance with increasing amplitude noise intensity V_N ($f_c=2$ kHz) were observed at: (**a**) $T=35$ °C ($\sigma_H=1.88$) and $s_a=0.80$, (**b**) $T=30$ °C ($\sigma_H=1.60$) and $s_a=0.80$, (**c**) $T=30$ °C and $s_a=0.96$, and (**d**) $T=30$ °C and $s_a=0.98$. The ISR in (**b**) was more clearly observed than in (**a**). Moreover, the ISR in (**b**) completely disappears at different values of s_a in (**c**) and (**d**).

power spectra[31]. If feasible, the initialized noise should be appropriately tuned for noise-related applications. Computer-programmed noise with adjusted steepness may be a feasible alternative option for such applications.

Experimental tests for the Helfrich conductivity and the steepness

To confirm the effects of the internal and external parameters (σ_H and s), experimental tests were conducted in a planarly-aligned cell [$\boldsymbol{n}_0=(1, 0, 0)$] using an NLC (MBBA) with $d=50$ μm. Initially, an EC (Williams domain) was observed at $V=5.9$ V, $f=500$ Hz, and $T=35$ °C. Subsequent pattern changes were observed with increasing amplitude noise intensity V_N ($f_c=2$ kHz and $s_a=0.80$), as shown in Fig. 9a. The optical intensity contrast of the pattern corresponding to the performance of EC slightly decreased at $V_N=2.0$ V and then increased with increasing V_N, resulting in high intensity contrast at $V_N=4.7$ V. This indicates the presence of a weak ISR, suggesting a small SNR. The experiment was repeated at a different temperature ($T=30$ °C) corresponding to a different value of the Helfrich conductivityσ_H, as shown in Fig. 9b. The EC nearly disappeared at $V_N=2.0$ V and then reappeared at $V_N=3.4$ V, indicating the presence of a clear ISR. Additionally, the pattern changes were quantified

as the contrast intensity I_C in Fig. 10. I_C was determined by averaging the optical intensity difference between minimal and maximal peaks in each pattern. For instance, the pattern observed at 4.7 V in Fig. 9a has 15 maximal peaks, indicating upward and downward flows corresponding to the deviation angle φ of the director in the EC [Fig. 1 and Eqs. (1) and (2)]. The curves (a) and (b) in Fig. 10 correspond to the pattern changes in Fig. 9a and b, respectively. The inverted bell-shaped $I_C(V_N)$ indicating ISR is found in both (a) and (b). Notably, the $I_C(V_N)$ curve (b) for $\sigma_H = 1.60$ ($T = 30$ °C) is more pronounced than the curve (a) for $\sigma_H = 1.88$ ($T = 35$ °C), suggesting a clear ISR. This ISR completely disappeared at higher temperatures ($T > 37$ °C; $\sigma_H = 2.02$) (i.e., higher σ_H). These results are qualitatively consistent with the variation of $h(\phi_N = 0)$ shown in Fig. 3; h decreases with increasing σ_H (or T). The experimental results clearly demonstrate the effect of the internal parameter (σ_H).

Similarly, successive pattern changes were observed at $T = 30$ °C ($\sigma_H = 1.60$) under amplitude noises with different values of the steepness $s_a = 0.96$ (Fig. 9c) and $s_a = 0.98$ (Fig. 9d). Compared to the ISR observed in Fig. 9b ($s_a = 0.80$), the ISR completely disappears in Figs. 9c and d. In these cases, the EC forms patterns with higher optical intensity with respect to V_N. Consequently, the $I_C(V_N)$ curves (c) and (d) do not exhibit the inverted bell-shaped feature seen in Fig. 10. These results are qualitatively consistent with the variation of $h(\phi_N = 0)$ shown in Fig. 5; h decreases with increasing s_a, and then may reach to $h = 0$ (i.e., disappearance of ISR). Likewise, applying phase noises with different steepness s_p may induce a similar effect on SR. This indicates that steepness plays a crucial role in the emergence of ISR and SR.

Discussion and conclusion

Over the past four decades, SR has undergone intensive investigation as a counterintuitive phenomenon and has found extensive application across various fields due to its utilization of noise[21,39,40]. Recent studies[18,28] have proposed that phase noise, which is often overlooked, plays a substantial role in the emergence of SR and ISR when combined with conventional amplitude noise. Additionally, it was observed that the spectral colorization of noise is crucial for controlling SR and ISR[17,18,28]. Exploring these constructive aspects of noises, this study investigated the practical methods for controlling SR and ISR and their transition by manipulating the internal and external parameters. In the current experimental setup, the Helfrich conductivity (σ_H) and the noise power-spectrum steepness (s_a and s_p) were utilized as the internal and external parameters, respectively. By varying the internal (material) parameter, the performance levels of both resonances (denoted as h in Fig. 2a) can be modulated. Moreover, it was found that colored noises enabled the control not only of the typical SR effect (maximal performance) but also of the inverse ISR effect (minimal performance).

Conversely, the performance levels of both resonances can also be controlled when adjusting the external (noise) parameter. However, the impact of the steepness of the phase noise spectra differed markedly from that of the amplitude noise spectra. Specifically, the characteristic noise intensity (denoted as ϕ_N^* in Fig. 2b) for the transition from ISR to SR exhibited a smooth decrease with the amplitude noise steepness (Fig. 6). In contrast, it displayed a smooth increase with the phase noise steepness (Fig. 8). These contrasting behaviors highlight the effectiveness of combining both types of noises for the precise control of performance levels and the transition (denoted as $h = 0$) between SR and ISR.

The current findings reveal a typical behavior of the EC threshold (Fig. 2a) observed under fixed colored noises at their respective cutoff frequencies. Internal and external parameters can influence the level of performance and the transition from ISR to SR depending on these cutoff frequencies (i.e., f_{ca} and f_{cp}), which exhibit

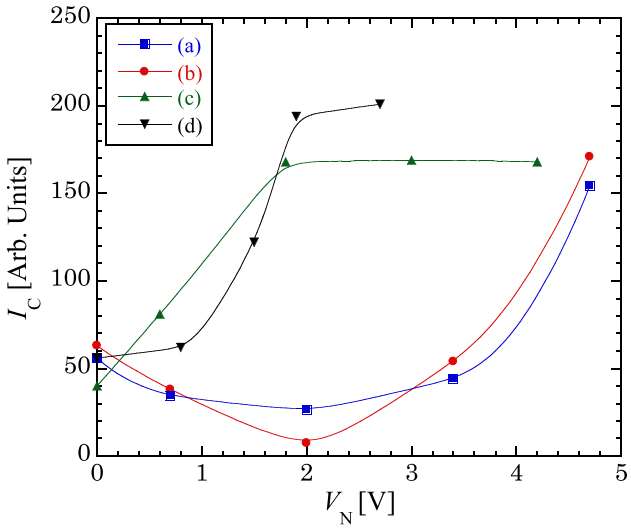

Fig. 10. Noise intensity V_N-dependent contrast intensity I_C of the pattern changes shown in Fig. 9. From the output performance (I_C) corresponding to the signal-to-noise ratio (SNR), ISR is observed in (**a**) and (**b**), with (**b**) exhibiting a deeper inverted bell-shaped curve than (**a**). ISR is not observed in (**c**) and (**d**). I_C was calculated using the minimal and maximal peaks indicating upward and downward flows in the EC patterns shown in Fig. 9.

distinct behaviors as outlined in a recent study[18]. For instance, slight variations in these parameters may induce both resonances even under conditions where noise intuitively exhibits no SR and ISR. Therefore, one can more effectively control SR, ISR, and their transition to meet specific requirements by precisely adjusting the system parameters under investigation.

Finally, the underlying mechanism behind the current results, particularly the outcomes related to steepness, is worth mentioning. In the Carr–Helfrich mechanism of AC-driven EC[32,34,36,41], the collective influence of electric noises on the AC field can substantially impact EC occurrence by affecting the motion of electric charges (specifically, the flow-induced torque to the director opposing the electro-elastic restoring torque to it), consequently altering the EC threshold V_c. Typically, white amplitude and phase noises decrease V_c due to random fluctuations contrasting with the sinusoidally alternating signal. However, appropriately colored amplitude and phase noises can modulate the AC signal to facilitate EC induction. Therefore, in the case of colored noises, the active attenuation (frequency) band (Fig. 1b) may play a crucial role in determining V_c alongside the conventional pass (frequency) band. In essence, the steepness, indicating the degree of the attenuation band, can influence the variation of V_c. However, the roles of amplitude and phase noises differ; one may suppress EC (i.e., stabilization effect), while the other may promote EC (i.e., destabilization effect), depending on the degree of the pass band (i.e., the cutoff frequency). Consequently, when both noises are combined, a certain interplay between noise-induced stabilization and destabilization effects on EC underlies the emergence of SR, ISR, and their transition. Phase noise (and its steepness) predominantly affects SR (Fig. 7). In contrast, amplitude noise (and its steepness) predominantly affects ISR (Fig. 5). More importantly, in amplitude noise, a smaller steepness (i.e., wider attenuation band) results in a greater height ($|h|$, i.e., better output performance from ISR). Similarly, in phase noise, a smaller steepness (i.e., wider attenuation band) leads to a greater height ($|h|$, i.e., better output performance from SR). Furthermore, the transition between SR and ISR can be controlled by varying the steepness of both noises. This implies that the attenuation band is susceptible to the appearance and disappearance of EC, consequently leading to the emergence of SR and ISR.

The current findings indicate that finely adjusting amplitude and phase noises can be highly beneficial for controlling SR and ISR in noise-related applications. Specifically, it is demonstrated that the steepness (i.e., the edge effect) of noise power spectra can influence the emergence and transition of both resonances[31,42]. Furthermore, varying appropriate internal parameters of the system may yield unexpected results for both resonances. The approach employed in this study holds promise for utilization in electrical applications where both amplitude and phase noises can be finely tuned. For instance, in sensing technology[43,44], finely tuned noises could enhance the performance of sensors in detecting weak signals. In biotechnology[39,45], the same principles could improve the accuracy of bio-detection systems. Moreover, our findings could be applied to neural networks for optimizing signal processing[12,13]. By tuning these noise parameters, our research can provide significant advancements across these fields, following the principles of SR and ISR demonstrated in previous studies. The ability to control the transition between both resonances may offer more effective methods to achieve the desired performance outcomes based on specific requirements.

Methods

Numerical calculation

The discrete fourth-order Runge–Kutta method within the general-purpose software MATLAB R2023b[46] was employed to determine the threshold voltage V_c of EC based on the governing Eqs. (1) and (2) for the Carr–Helfrich mechanism[32,36,41]. Specifically, V_c was determined as the lowest value V in the numerical loop, with an increment of ΔV (= 0.1 V in this study), for which the director angle φ [see Fig. 1a] does not relax to zero due to instability[36]. Thus, through linear stability analysis, V_c was automatically established by confirming $\varphi(t) \rightarrow 0$ or ∞ (for $t \rightarrow \infty$) within a margin of error of $\pm \Delta V$ [V]. In this study, the primary control parameters, represented by colored Gaussian noises with cutoff frequencies f_{ca} and f_{cp} and steepness s_a and s_p, were provided by a frequency filtering program in the software. The material parameters for the NLC (i.e., MBBA) utilized in this study align with those detailed in our recent report[18].

Tuning noise in numerical examination and for an experimental approach

In numerical studies, colored noises that are generated from computer-programmed noise filters must undergo tests to confirm their power spectra. For instance, the frequency filtering program integrated into general-purpose software like MATLAB, utilized in this study, provides two types of low-pass filters, i.e., finite impulse response and infinite impulse response, exhibiting distinct power spectra at the same cutoff frequency and steepness. This observation highlights the differences in noise characteristics between the two types of low-pass filters. Depending on the research subject, these differences may have noticeable effects. On the other hand, in experimental setup, noise generators or noise filters are typically employed for noise-related studies and applications. The details of colored noises can be adjusted through the built-in features of each generator and noise filter. For example, the programmable noise filters (NF, 3628) of this study offer maximum flat ($s = 0.96$) and phase linear ($s = 0.98$) low-pass filters. Although their cutoff frequency is set at the same values, their power spectra exhibit slight differences, indicating varying steepness.

Data availability

The data supporting the findings of this study are available from the corresponding author upon reasonable request.

Received: 24 June 2024; Accepted: 2 September 2024
Published online: 18 September 2024

References

1. Benzi, R., Sutera, A. & Vulpiani, A. The mechanism of stochastic resonance. *J. Phys. A* **14**, L453 (1981).
2. Gutkin, B., Jost, J. & Tuckwell, H. C. Inhibition of rhythmic neural spiking by noise: the occurrence of a minimum in activity with increasing noise. *Naturwissenschaften* **96**, 1091 (2009).
3. Benzi, R., Parisi, G., Sutera, A. & Vulpiani, A. Stochastic resonance in climate change. *Tellus* **34**, 10 (1982).
4. Bhar, B., Khanna, A., Parihar, A., Datta, S. & Raychowdhury, A. Stochastic resonance in insulator-metal-transition systems. *Sci. Rep.* **10**, 5549 (2020).
5. Dodda, A. *et al.* Stochastic resonance in MoS_2 photodetector. *Nat. Commun.* **11**, 4406 (2020).
6. Hohmann, W., Müller, J. & Schneider, F. W. Stochastic resonance in chemistry. *J. Phys. Chem.* **100**, 5388 (1996).
7. Suzuki, Y. & Asakawa, N. Stochastic resonance in organic electronic devices. *Polymers* **14**, 747 (2022).
8. Douglass, J. K., Wilkens, L., Pantazelou, E. & Moss, F. Noise enhancement of information transfer in crayfish mechanoreceptors by stochastic resonance. *Nature* **65**, 337 (1993).
9. Russell, D. F., Wilkens, L. A. & Moss, F. Use of behavioral stochastic resonance by paddle fish for feeding. *Nature* **402**, 291 (1999).
10. Simonotto, E. *et al.* Visual perception of stochastic resonance. *Phys. Rev. Lett.* **78**, 1186 (1997).
11. Roy, P. K. & Rallabandi, V. P. S. Magnetic resonance imaging (MRI) enhancement using stochastic resonance. *Magn. Reson. Imaging* **28**, 1361 (2010).
12. Gluckman, B. J. *et al.* Stochastic resonance in a neuronal network from the mammalian brain. *Phys. Rev. Lett.* **77**, 4098 (1996).
13. Kai, S. & Mori, T. Noise-induced entrainment and stochastic resonance in human brain waves. *Phys. Rev. Lett.* **88**, 218101 (2002).
14. Uzuntarla, M., Cressman, J. R., Ozer, M. & Barreto, E. Dynamical structure underlying inverse stochastic resonance and its implications. *Phys. Rev. E* **88**, 042712 (2013).
15. Zamani, A., Novikov, N. & Gutkin, B. Concomitance of inverse stochastic resonance and stochastic resonance in a minimal bistable spiking neural circuit. *Commun. Nonlinear Sci. Numer. Simulat.* **82**, 105024 (2020).
16. Touboul, J. D., Staver, A. C. & Levin, S. A. On the complex dynamics of savanna landscapes. *Proc. Natl. Acad. Sci. U.S.A.* **115**, E1336 (2018).
17. Huh, J.-H. Inverse stochastic resonance in electroconvection by multiplicative colored noise. *Phys. Rev. E* **94**, 052702 (2016).
18. Huh, J.-H., Shiomi, M. & Miyagawa, N. Control of stochastic and inverse stochastic resonaces in a liquid-crystal electro convection system using amplitude and phase noises. *Sci. Rep.* **13**, 16883 (2023).
19. Zhang, X.-J., Qian, H. & Qian, M. Stochastic theory of nonequilibrium steady states and its applications. *Part I. Phys. Rep.* **510**, 1 (2012).
20. Torres, J. J., Uzuntarla, M. & Marro, J. A theoretical description of inverse stochastic resonance in nature. *Commun. Nonlinear Sci.* **80**, 104975 (2020).
21. Gammaitoni, L., Hanggi, P., Jung, P. & Marchesoni, F. Stochastic resonance. *Rev. Mod. Phys.* **70**, 223 (1998).
22. Jia, Y., Zheng, X., Hu, X. & Li, J. Effects of colored noise on stochastic resonance in a bistable system subject to multiplicative and additive noise. *Phys. Rev. E* **63**, 031107 (2001).
23. Nicolis, G. & Altares, V. A new method of analysis of the effect of weak colored noise in nonlinear dynamical systems. *J. Stat. Phys.* **46**, 191 (1987).
24. Gammaitoni, L., Marchesoni, F., Menichella-Saetta, E. & Santucci, S. Multiplicative stochastic resonance. *Phys. Rev. E* **49**, 4878 (1994).
25. Seki, K. & Barzykin, A. V. Stochastic resonance driven by Gaussian multiplicative noise. *Europhys. Lett.* **40**, 117 (1997).
26. Huh, J.-H. Influence of external noise on various electrohydrodynamic instabilities in a nematic liquid crystal. *J. Phys. Soc. Jpn.* **81**, 104602 (2012).
27. Chowdhury, A., Barbay, S., Clerc, M. G., Robert-Philip, I. & Braive, R. Phase stochastic resonance in a forced nanoelectromechanical membrane. *Phys. Rev. Lett.* **119**, 234101 (2017).
28. Huh, J.-H., Yano, Y. & Miyagawa, N. Phase noise can induce stochastic resonance?. *J. Phys. Soc. Jpn.* **88**, 063001 (2019).
29. Castro, F. J., Kuperman, M. N., Fuentes, M. & Wio, H. S. Experimental evidence of stochastic resonance without tuning due to non-Gaussian noises. *Phys. Rev. E* **64**, 051105 (2001).
30. Chen, Y.-F., Wang, K.-K., Ye, H. & Wang, Y.-J. Impact of non-gaussian noise and time delay on stability and stochastic resonance for a FitzHugh-Nagumo neural system subjected to a multiplicative periodic signal. *Fluct. Noise Lett.* **23**, 2450002 (2024).
31. Fantini, D. A. & Emmerich, D. S. Edge effects on frequency discrimination of tones presented in low- and high-pass noise backgrounds. *J. Acoust. Soc. Am.* **82**, 1593 (1987).
32. Prost, J. & de Gennes, P. G. *The Physics of Liquid Crystals* (Claerendon, 1993).
33. Mishali, M. & Eldar, Y. C. From theory to practice: Sub-Nyquist sampling of sparse wideband analog signals. *IEEE J. Sel. Top. Sig. Proc.* **4**, 375 (2010).
34. Kawakubo, T., Yanagita, A. & Kabashima, S. External noise effect on the onset of Williams domain in nematic liquid crystals. *J. Phys. Soc. Jpn.* **50**, 1451 (1981).
35. Williams, R. Domains in liquid crystals. *J. Chem. Phys.* **39**, 384 (1963).
36. Smith, I. W., Galerne, Y., Lagerwall, S. T., Dubois-Violette, E. & Durand, G. Dynamics of electrohydrodynamic instabilities in nematic liquid crystals. *J. Phys. (Paris)* **36**, C1-237 (1975).
37. Huh, J.-H. Noise-induced threshold shift and pattern formation in electroconvection by controlling characteristic time scales. *Phys. Rev. E* **84**, 025302 (2011).
38. Huh, J.-H. & Kai, S. Colored noise-induced threshold shifts and phase diagrams in electroconvections. *J. Phys. Soc. Jpn.* **83**, 063601 (2014).
39. McDonnell, M. D. & Abbott, D. What is stochastic resonance? Definitions, misconceptions, debates, and its relevance to biology. *PLoS Comput. Biol.* **5**, e1000348 (2009).
40. Budrikis, Z. Forty years of stochastic resonance. *Nat. Rev. Phys.* **3**, 771 (2021).
41. Eber, N., Salamon, P. & Buka, A. Electrically induced patterns in nematics and how to avoid them. *Liq. Cryst. Rev.* **4**, 101 (2016).
42. Jurado, C. A., Pedersen, C. S. & Møller, H. Auditory filters at low-frequencies: Filter shape in the range 50 Hz to 1000 Hz. In *8th European Cence on Noise Control 2009 (EURONOISE 2009)* (eds Jurado, C. A. *et al.*) (Institute of Acoustics, 2009).
43. Saha, A. A. & Anand, G. V. Design of detectors based on stochastic resonance. *Sig. Proc.* **83**, 1193 (2003).
44. Li, Q. & Li, Z. A novel sequential spectrum sensing method in cognitive radio using suprathreshold stochastic resonance. *IEEE Trans. on Vehicular Tech.* **63**, 1717 (2014).
45. Hänggi, P. Stochastic resonance in biology: How noise can enhance detection of weak signals and help improve biological information processing. *ChemPhysChem* **3**, 285 (2002).
46. Shampine, L. F. & Reichelt, M. W. The MATLAB ode suite. *SIAM J. Sci. Comput.* **18**, 1 (1997).

Acknowledgements

This work was supported by JSPS KAKENHI Grant Number 22K03470. The authors would like to thank Enago (www.enago.jp) for the manuscript review and editing support.

Author contributions

J.-H.H. conceived the research and wrote the paper. T.H. and Y.S. performed the numerical analysis. J.-H.H. and Y.S. carried out the experimental examination. All authors contributed to all aspects of this work.

Competing interests

The authors declare no competing interests.

Additional information

Correspondence and requests for materials should be addressed to J.-H.H.

Reprints and permissions information is available at www.nature.com/reprints.

Publisher's note Springer Nature remains neutral with regard to jurisdictional claims in published maps and institutional affiliations.